PHYSICAL REVIEW B VOLUME 37, NUMBER 17 15 JUNE 1988-I

Adsorption and growth of Sn on Si(100) from synchrotron photoemission studies

D. H. Rich, T. Miller, A. Samsavar, H. F. Lin,* and T.-C. Chiang
Department of Physics and Materials Research Laboratory, University of Illinois at Urbana-Champaign,
1110 West Green Street, Urbana, Illinois 61801
(Received 11 December 1987)

Photoemission spectroscopy was used to study the initial growth and interaction of Sn on Si(100). The as-deposited surfaces were annealed at about 550 °C, generating the following coverage-dependent reconstructions: $c(4\times4)$, (6×2), $c(8\times4)$, and (5×1). Changes in the Si $2p$ core-level line shape were identified as the selective modification of Si surface dimer atoms by the presence of Sn adatoms. A relative measure of the Sn-adatom–Si-substrate interaction is presented by quantification of the average number of Si surface sites modified in the presence of a Sn adatom for various coverages. The Sn $4d$ core-level spectra revealed two components for Sn coverages below 1 monolayer (ML), indicating the existence of two inequivalent Sn sites, whose relative occupancy is seen to vary with coverage. The Sn $4d$ core level for the majority sites roughly follows the movement of the Fermi level within the band gap of Si for increasing Sn coverages, while that for the minority sites remains at a constant binding energy relative to the Si valence-band maximum. Implications concerning the structure of the Sn overlayer are discussed. The Sn-induced band bending and the Schottky barrier height are obtained. Photoemission from the valence bands near the Fermi level shows that the Sn-covered Si(100) surface has little density of states at the Fermi level for coverages below 1 ML.

I. INTRODUCTION

Difficulties in obtaining the epitaxial growth of high-quality films on semiconductor substrates often stem from an inadequate understanding of the initial interaction of adsorbates with the substrate. Similarly, studies of interface electronic-barrier formation often lack the critical band-bending information that can only be acquired through low-coverage studies of overlayers on the substrates. The initial nucleation, growth morphology, intermixing, and reaction of adsorbates on semiconductor substrates are commonly monitored with the medium-range probe of photoemission spectroscopy, which can supply crucial information concerning the electronic properties and chemical composition of the surface atomic layer and the first few subsurface layers. In particular, the Sn-on-Si(100) system represents an important interfacial system involving elements of the same nominal chemical valence of the group-IV family of the Periodic Table. Bulk Sn in its allotropic form of gray tin is semiconducting with a small energy gap and has the same diamond structure as Si, while white tin, occurring at temperatures above 13 °C, is metallic. Although high-quality thick gray-tin films have been epitaxially grown on the lattice-matched (100) surfaces of InSb and CdTe, no such success has been reported for the Si substrates which are not lattice-matched to either form of Sn.[1] For comparison, high-quality growth of Ge films on Si has been reported, even though there is also a significant lattice mismatch in this case.[2] Hence, from a fundamental viewpoint, it will be interesting to investigate the Sn-Si(100) interface on an atomic scale.

The clean Si(100) (2×1) surface has been extensively studied by electron and He diffraction; higher-ordered reconstructions of (2×2) and $c(4\times2)$ have been observed.[3–5] A variety of theoretical models have been proposed to explain such structures.[6–8] Recently, a scanning-tunneling-microscopy (STM) study of Si(100) (2×1) has revealed that the surface reconstruction is a consequence of the formation of dimers.[9] Both buckled and nonbuckled dimers are present in approximately equal numbers, while a small portion of the surface suffers from defects, most of which are related to missing dimers. In addition, a recent electron-diffraction study has shown that phases with $(2\times n)$ structure $(6<n<10)$ can be formed on the clean surface by rapid quenching from high temperatures.[10] In the present study, only surfaces with a nominal (2×1) reconstruction were investigated.

Until recently, relatively little work has been documented concerning the behavior of Sn on Si(100). Kuwata *et al.* first observed a Sn-induced $c(8\times4)$ and (5×1) reconstruction on Si(100) with electron diffraction.[11] A rather extensive surface phase diagram has been characterized by Ueda and Kinoshita, who reported the existence of $c(4\times4)$, (6×2), $c(8\times4)$, and (5×1) structures for various coverages and proper annealing temperatures.[12] High- and low-energy electron diffraction (HEED and LEED) along with Auger-electron spectroscopy were employed in this study.

Because core-level binding energies are dependent upon the local atomic environment, high-resolution photoemission spectra may contain information concerning the occupation of atoms in inequivalent sites. Since the local atomic environment of a crystal is often considerably different at the surface than in the bulk, we can expect that surface atoms will generally exhibit different core-level binding energies than atoms in the bulk. Consequently, surface core-level binding-energy shifts have been observed in many cases.[13,14] Also, since the addition of an overlayer material will alter the local atomic environment of certain surface sites, high-resolution core-level photoemission from both the substrate and adsorbate core levels can be used to examine the modification of such sites, often providing vital clues leading to a deduction of the adsorbate-substrate interface structure. For elemental semiconductors, previous studies have suggested that the surface core-level shifts can be related to the presence of dangling bonds and surface-reconstruction effects.[15] A number of core-level studies of the Si and Ge surfaces employing adsorbates varying in electronegativity have yielded information leading to a semiquantitative connection between the effective charge transfer and the core-energy shift induced by adsorption.[13,16–18]

In the present study the Sn-Si(100) interface was investigated by analyzing high-resolution photoemission spectra from the Sn 4*d* and Si 2*p* core levels and valence bands. By simultaneously examining changes in the substrate and overlayer core levels, site-specific information regarding the substrate-adsorbate coordination can be obtained. Specifically, the number of Si surface sites altered in the presence of a Sn adatom is obtained. The Sn adatoms are found to occupy two distinct types of surface sites which possess differences in binding energy and atomic environment. In addition, changes in the density of states (DOS) near the Fermi level are examined by photoemission from the valence bands for different coverages. From these results, specific details regarding the Sn-Si interaction and site occupation are concluded. Structural models which correlate with the photoemission data are discussed.

II. EXPERIMENTAL DETAILS

The photoemission experiments were carried out using synchrotron radiation from the University of Illinois beam line on the 1-GeV storage ring at the Synchrotron Radiation Center of the University of Wisconsin–Madison at Stoughton, Wisconsin. Light from the ring was monochromatized by an "Extended Range Grasshopper" monochromator.[19] A double-pass cylindrical-mirror analyzer was used to detect electrons emitted from the sample. The overall instrumental resolution was typically 0.2–0.3 eV. The sample Fermi level was determined by observing emission from the Fermi edge of a polycrystalline Au sample in electrical contact with the Si sample.

The *n*-type Si(100) samples which came from a commercially polished wafer stock having room-temperature resistivities of 10–15 Ω cm were cut into rectangles having the approximate dimensions of $14\times5\times0.25$ mm^3. The wafers were then etched in a 35 vol % nitric acid solution for 5 min and then rinsed with distilled water. The Si samples were then mounted on sample holders with tantalum supports. Heating the sample was accomplished by passing a current through the sample and the temperature was monitored with an infrared pyrometer. The samples were cleaned by thermal annealing at about 1100 °C for 10 s in our vacuum chamber which has a base pressure of about 1×10^{-10} Torr.

The surface reconstruction of the clean Si(100) surface was checked by high-energy electron diffraction (HEED), which revealed a sharp two-domain (2×1) pattern and occasionally a small mixture of (2×2). The Sn overlayers on Si(100) were prepared by evaporation from an electron-beam-heated tungsten crucible containing 99.999%-pure elemental Sn. The rate of deposition was monitored using a quartz crystal-thickness monitor and was maintained at about 1 monolayer (ML) per minute. In this paper 1 ML of Sn is defined as 6.8×10^{14} atoms/cm^2, which is the site-number density for the unreconstructed Si(100) surface. For each coverage, Sn was deposited upon a freshly cleaned Si(100) (2×1) substrate at temperatures between 150 and 200 °C. The as-deposited surfaces were annealed at 550 °C for 2 min and allowed to cool to 100–150 °C before the measurements began. This procedure produced the coverage dependent two-domain reconstructions: $c(4\times4)$, (6×2), $c(8\times4)$, and (5×1), in agreement with previous results.[12] Photoemission spectra were taken for the Si 2*p* and Sn 4*d* core levels and valence bands. In order to help differentiate the photoemission contribution of the Si surface atoms from those of the substrate layers, two different energies 140 and 108 eV were used. The Sn 4*d* core and the valence bands were examined with an 80-eV photon energy.

III. RESULTS

A. HEED

The reconstruction phases of the Sn-deposited Si(100) surfaces depend on coverage and annealing temperature. The Sn-covered samples were annealed as described above, and failure to anneal the samples resulted in an increasingly diffuse (2×1) HEED pattern for increasing coverages, indicating that deposited Sn was disordered for low surface temperatures. A phase diagram for the annealed surface is shown in Fig. 1. For coverages $0\leq\Theta<0.2$ ML, a (2×1) reconstruction is observed, which becomes more diffuse as Θ approaches 0.2 ML, in-

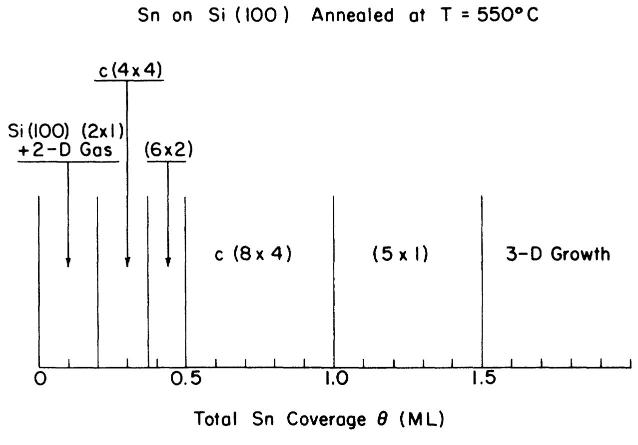

FIG. 1. The surface phase diagram for Sn on Si(100).

dicating the Si(100) (2×1) substrate coexists with a significant amount of disorder introduced by the Sn adsorption. For higher coverages, the various reconstructions observed are indicated. When $\Theta>1.5$ ML, significant intensity modulation occurs along the $\frac{1}{5}$-order HEED streaks when the incident-electron beam is along the [011] direction; this observation indicates three-dimensional growth. These results are consistent with those of Ref. 12.

B. Si 2*p* core level

To differentiate the surface and bulk contributions of the Si 2*p* core level in the photoemission spectra, two photon energies, 140 and 108 eV, are used, giving rise to surface- and bulk-sensitive spectra, respectively. The surface-sensitive spectra (140 eV) for clean and some Sn-covered surfaces are shown in Fig. 2. The spectrum for the clean surface shows an additional hump on the lower-binding-energy side of the main spin-orbit-split component, which is the result of a distinct surface core-level shift. This hump is also present in the bulk-sensitive spectrum ($h\nu=108$ eV and not shown), but with a much reduced intensity.[20] The decomposition of the spectra into the bulk and surface contributions have been discussed in a previous publication.[16] Briefly, both the bulk- and surface-sensitive spectra are fitted simultaneously by a model function consisting of a bulk component and a replicated and shifted surface component with a different intensity riding on a smooth cubic polynomial background, and each component consists of a pair of Voigt line shapes separated by the spin-orbit splitting.[21] The result of the deconvolution is indicated in the figure by the dotted curve for the bulk contribution and the dashed curve for the surface contribution, both offset in the vertical direction for clarity. The solid curve running through the data points is the overall fit, and the cubic background function is not shown. The relevant fitting parameters can be found in a previous publication.[16] The relative binding-energy scale in Fig. 2 is referred to the bulk contribution of the Si $2p_{3/2}$ core level, which is at 99.13 ± 0.05 eV below the valence-band maximum (VBM) of Si. This energy reference is an intrinsic property of the Si substrate and is independent of the Sn coverage. For the clean Si(100) (2×1) surface, the Fermi level is pinned at 0.41 ± 0.05 eV above the VBM, which is consistent with a previous report.[20] Both these energy references have been determined by comparing the bulk Si 2*p* core-level binding energies of the clean Si(100) (2×1) and Si(111) (7×7) surfaces with respect to the Fermi level, and using the known Fermi-level-pinning position for the (7×7) surface, which is at 0.63 eV above the VBM.[22]

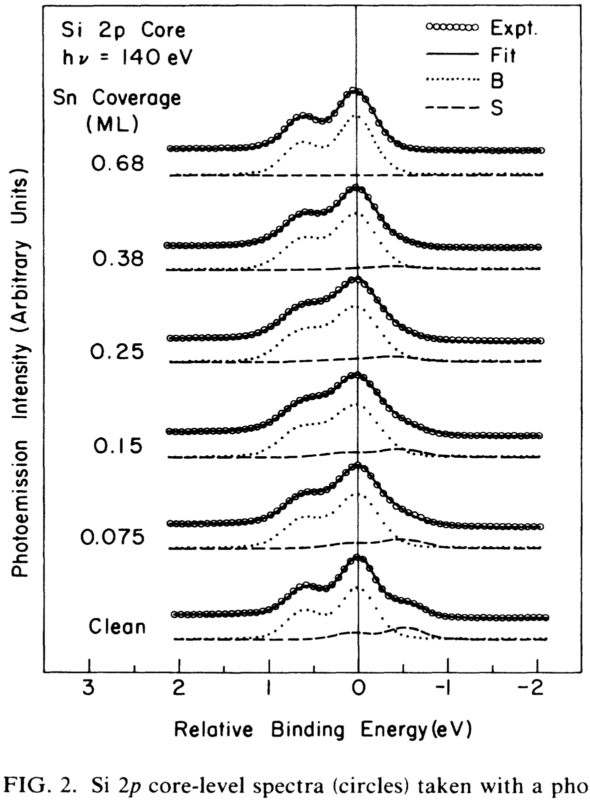

FIG. 2. Si 2*p* core-level spectra (circles) taken with a photon energy of 140 eV for the clean Si(100) (2×1) and Sn-covered Si(100). The coverages of Sn are indicated. The solid curves are the result of a fit to the data. The decomposition of the spectra into the bulk (*B*) and surface (*S*) contributions are shown by the dotted and dashed curves, respectively. The relative binding-energy scale is referred to the Si $2p_{3/2}$ core-level component of the bulk contribution.

The surface- and bulk-sensitive Si 2*p* core-level spectra for the Sn-covered surfaces were analyzed in the same fashion as for the clean case; only some of the surface-sensitive spectra are shown in Fig. 2. The intensity of the surface component is seen to decrease with increasing Sn coverages, and its position remains shifted by about 0.5 eV towards lower binding energies with respect to the bulk component. The highest-Sn coverage which exhibits a barely detectable surface component is about 0.45 ML. The only other significant Sn-induced change in the Si 2*p* core-level line shapes is a 10–20 % increase in the Gaussian width, most likely a result of inhomogeneous broadening and small unresolved shifts. (In the fit, the Lorentzian width was constrained to be the same as for the clean case.) In the photoemission spectra, the bulk Si $2p_{3/2}$ component moves toward lower binding energies with respect to the Fermi level for increasing Sn coverages, which is indicative of the typical band bending that is observed for various metal-semiconductor systems. This band-bending shift does not show in Fig. 2, because the spectra are aligned with respect to the VBM (with a constant offset). From the band bending deduced from the core-level data, the position of the Fermi level relative to the band edges in Si is shown in Fig. 3 as a function of Sn coverage. The Sn-induced change in the Fermi-level position is about 0.4 eV towards the VBM for $\Theta>1$ ML; thus the final Fermi-level position is approximately at the VBM. The Schottky-barrier height for the *n*-type sample is roughly equal to the Si band gap.

From the intensity ratio between the surface and bulk components, the relative number of Si atoms contributing to the surface component for various Sn coverages can be obtained from the usual escape-depth model, provided the escape depth or, equivalently, the clean-surface cover-

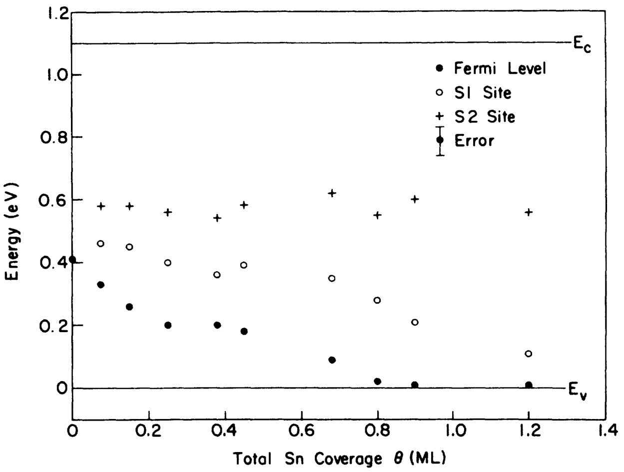

FIG. 3. The energy positions of the Fermi level (●) and the Sn $4d_{5/2}$ core-level components of the $S1$ site (○), and the $S2$ site (+) relative to the Si band edges for various Sn coverages. The $S1$- and $S2$-site binding energies have been offset by −24.05 and −24.90 eV, respectively, to illustrate the correlations with the gap and Fermi-level positions. E_v and E_c denote the valence-band maximum and conduction-band minimum of Si, respectively.

age is known.[16] The number of dimer atoms on the clean Si(100) (2×1) surface which contribute to the surface component has been determined by performing an *in situ* comparison with the Si(111) (7×7) surface.[16,23] By correlating distinct features of the (7×7) spectrum with the structural features of the (7×7) surface, which is known to have $\frac{12}{49}$ ML of "adatoms" on the surface,[24] the number of surface atoms which contribute to the Si(100) (2×1) surface component is determined to be 0.92±0.07 ML. The uncertainty here is the standard deviation over the 20 samples examined in this study. The surface-shifted component has been attributed to the surface dimer atoms, and the departure from 1 ML for a perfect (2×1) surface has been attributed to the presence of defects in the form of missing dimers observed by STM.

The reduction in the surface-component intensity for increasing Sn coverages is due to the bonding of Si surface atoms to Sn adatoms, resulting in a more bulklike environment for the Si surface atoms and hence a new core-level binding energy very close to the bulk value. From the analysis we have obtained the average number of Si surface atoms which have been converted to have a bulklike binding energy in the presence of each Sn atom for various coverages, which is hereafter referred to as the Sn-Si modification number. The result is shown in Fig. 4 as a function of Sn coverage up to about $\Theta=0.5$ ML; beyond this coverage the surface component has zero intensity. The uncertainty in the dimer-atom population on the clean surface leads to a systematic error of about 8% in the data points shown in Fig. 4; random fluctuations are due to limited experimental precision. The interpretation of this modification number depends strongly on the atomic environment experienced by each Sn atom. Thus model development must be deferred until after an examination of the Sn 4*d* core levels.

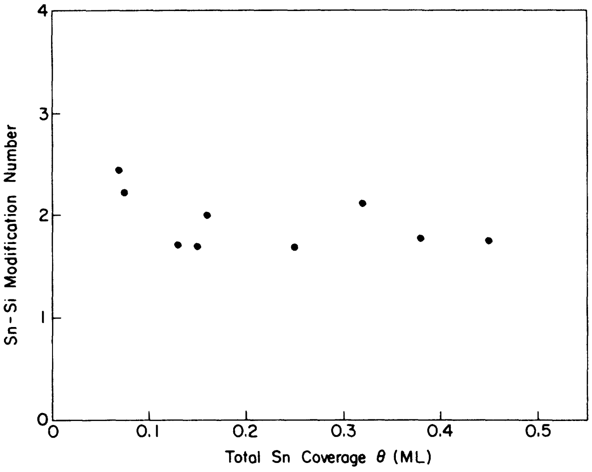

FIG. 4. The average number of Si surface atoms affected by a Sn adatom (the Sn-Si modification number), for various Sn coverages.

C. Sn 4*d* core level

Figure 5 shows the Sn 4*d* core-level spectra for various coverages, taken with 80 eV photon energy. The binding-energy scale is referred to the Fermi level. It is apparent from an inspection of the spectra that an addi-

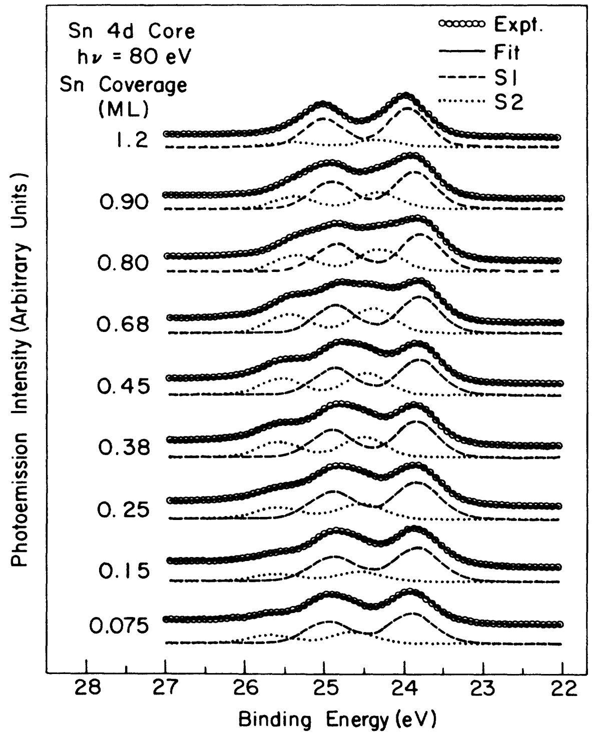

FIG. 5. The Sn 4*d* core-level spectra (circles) taken with a photon energy of 80 eV for various Sn coverages of Si(100). The solid curves are the result of a fit to the data. The decomposition into the $S1$ and $S2$ contributions are shown by the dashed and dotted curves, respectively. The binding-energy scale is referred to the Fermi level.

tional hump grows on the higher-binding-energy end of the main spin-orbit-split peak for increasing coverages in the range $0<\Theta<0.68$ ML. For $\Theta>0.68$ ML. this additional hump, as well as the intensity from the spin-orbit-split valley of the main peak, decreases noticeably. Hence, by this simple visual inspection, it is apparent that there are two distinct components. A detailed least-squares analysis similar to the one described above for the Si $2p$ core level has shown that the use of two components is sufficient to fit the data, and the addition of a third component does not improve the quality of the fit. The results of the fit and the components are indicated in Fig. 5 by various curves. The lower- and higher-binding-energy components are labeled $S1$ and $S2$, respectively. For all coverages, the Gaussian width, branching ratio, and spin-orbit splitting converged to 0.61 ± 0.05, 0.74 ± 0.02, and 0.105 ± 0.001 eV, respectively; the Lorentzian width was constrained to be equal to that (0.063 eV) obtained from the lowest coverage, $\Theta=0.019$ ML, which exhibited the narrowest overall width.

The binding energies of the $S1$ and $S2$ components depend on the Sn coverage; the energy positions of the Sn $4d_{5/2}$ core are shown in Fig. 3. In constructing this figure, the binding energies for $S1$ and $S2$ sites have been offset arbitrarily by -24.05 and -24.90 eV, respectively, to illustrate a comparison with the Fermi level position in the Si band gap for various Sn coverages. The relatively slow variation in energy accompanied with large changes in relative intensity of the $S1$ and $S2$ components suggest that the emissions giving rise to $S1$ and $S2$ are from two distinct sets of Sn adsorption sites on the Si(100) surface. The variation in intensity is then a direct measure of the relative population of each site (see below). It is apparent from Fig. 3 that the change in $S1$ binding energy closely parallels the Fermi-level shift relative to the gap, while the $S2$ binding energy is approximately a constant relative to the VBM.

The annealing of the as-deposited surfaces did not cause the Sn $4d$ signal to decrease, and the total integrated Sn $4d$ intensity is seen to increase linearly for coverages up to about 1 ML, indicating that both the $S1$ and $S2$ sites reside in the near-surface region, with no appreciable diffusion into the bulk Si crystal. From the relative intensities of the $S1$ and $S2$ components obtained from the fits to the Sn $4d$ core-level spectra, the contributions of the $S1$ and $S2$ sites to the Sn coverage are plotted versus the total Sn coverage in Fig. 6. For Sn coverages $\Theta<0.1$ ML, the $S1$- and $S2$-site populations are seen to increase linearly at different rates with roughly a factor-of-7 ratio between the $S1$ and $S2$ slopes. For $0.2<\Theta<0.68$ ML, during which the ordered structures appear, the $S1$ and $S2$ growth rates are nearly equal. For $\Theta>1$ ML, there is a significant decrease in the $S2$ growth rate with an accompanying increase in the $S1$ growth rate. However, there is some uncertainty in the analysis in this region due to the attenuation of photoelectrons emanating from the Sn sites residing in nonequivalent layers at the surface region. As will be discussed in Sec. IV, the $S2$ sites are believed to lie below the $S1$ sites, within one atomic layer, leading to the direction of the estimated correction bars illustrated in Fig. 6 due to self-attenuation. The magnitude of the corrections are based on a simple discrete-layer attenuation model using an estimated escape depth of 5 Å in Sn at 50 eV kinetic energy.

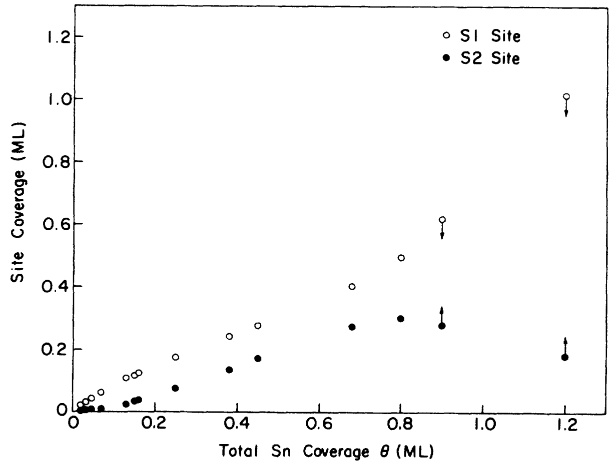

FIG. 6. The Sn $S1$- (○) and $S2$- (●) site coverages as a function of total Sn coverage. The sum of the $S1$ and $S2$ coverages is the total coverage. The arrows indicate possible corrections due to the attenuation of photoelectrons emanating from the $S2$ site by the $S1$ sites.

D. Valence bands

The valence-band photoemission spectra for various coverages, taken with 80 eV photon energy, are shown in Fig. 7. The binding-energy scale is referred to the Fermi

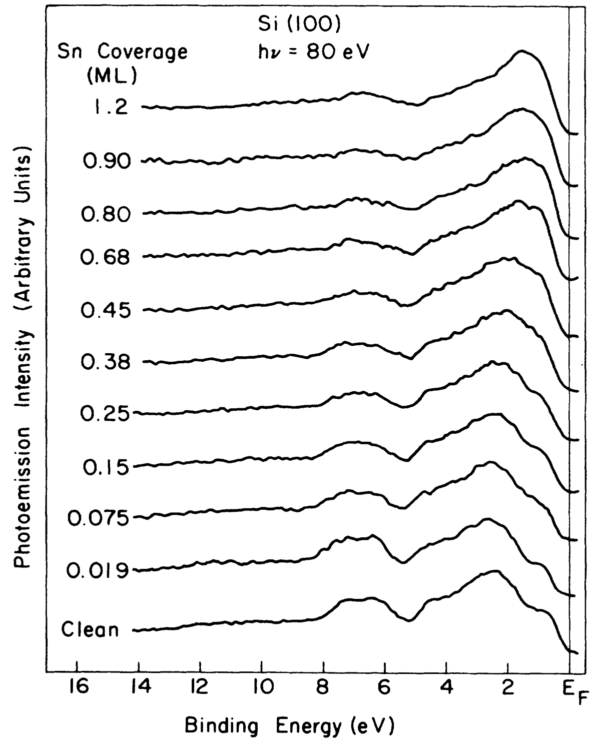

FIG. 7. Angle-integrated valence-band photoemission spectra taken with 80 eV photon energy for the Sn coverages shown. The energy scale is referred to the Fermi level.

level. These spectra should represent the DOS to a good approximation in our angle-integrated geometry.[21] The clean Si(100) surface exhibits a surface-state–derived feature at roughly 1 eV binding energy; this feature can be resolved clearly into two peaks in angle-resolved measurements.[25,26] The structures located 2–10 eV below the Fermi level are derived from the bulk valence bands.[21,26] By overlaying these spectra, one can detect an approximately uniform movement of these features towards the Fermi level for increasing Sn coverages, which is due to the band bending illustrated in Fig. 3. For the coverage $\Theta = 0.019$ ML, a comparison with the clean sample shows a decrease in the surface-state–emission intensity relative to the emission from the bulk-derived bands. However, the surface-state emission for higher coverages is masked by an increased slope near the VBM (typical of overlayer-induced states), preventing an accurate analysis of the alteration of the surface states. At all coverages $\Theta < 1$ ML, the emission intensity at the Fermi level is very low, indicating a low density of states.

IV. DISCUSSION AND MODEL DEVELOPMENT

A. The Sn-Si interaction at low coverages

Since Sn and Si have the same chemical valence and similar electronegativity, a variety of covalently bonded structural models can be proposed to explain the reconstructed structures observed for the different coverages. However, the number of structural models are considerably reduced when the constraints of the following photoemission data are imposed: the Sn-Si modification number, the $S2$- and $S1$-site occupation coverages, the $S2$ and $S1$ binding energies relative to the Fermi level as a function of coverage, and the Fermi-level position relative to the gap as a function of coverage.

From Fig. 6, about 90% of the Sn adatoms are $S1$-like for $\Theta < 0.1$ ML; therefore, we will ignore the $S2$ minority sites in the discussion in this subsection. Figure 4 shows that the Sn-Si modification number is close to 2 in this coverage range.

The principal mechanism leading to the -0.5-eV surface core-level shift in clean Si(100) (2×1) is an increased electron localization about the dimer atom resulting from its unsaturated dangling-bond orbital. The interaction of surface atoms with adsorbates can result in chemical shifts in the core-level binding energy. The chemical shifts are a rather short-ranged effect, being most important for the surface atoms in direct bonding with the adsorbate atoms. Recent studies of the Si(100) and Si(111) surfaces as well as other systems employing oxidation, chlorination, fluoridation, hydrogenation, and metallization have shown the chemical shift of the surface-atom core level to be intimately related to the electronegativity of the adsorbate species; the core-level shift is about 1 eV for highly ionic bonds.[13,16–18] Second-nearest-neighbor effects are smaller, being on the order of 0–0.2 eV, and in general cannot be resolved experimentally. In a recent study, it has been found that In adsorption on Si(100) results in a $+0.5$-eV shift of the surface Si $2p$ core, so that the Si surface atom after bonding to In shows essentially the bulk binding energy.[16] This behavior can be explained by the fact that In and Si have very similar electronegativities; thus the dangling bond of a Si atom on the clean Si(100) (2×1) surface is replaced by a covalent Si-to-In bond after In adsorption, resulting in a bulklike, fourfold-coordinated bonding environment for the Si surface atom. Since the electronegativity of Sn is also close to that of Si, it is not surprising to see again a $+0.5$-eV shift in the surface core-level binding energy of Si when Sn is adsorbed on Si.

A natural interpretation for the result is that the Sn atoms, being mostly dispersed on the surface (Fig. 1), from two Sn-to-Si bonds for each Sn adatom, so the Sn-Si modification number is 2. Such a twofold bonding characteristic suggests that each Sn adatom assumes a bicovalent s^2p^2 electronic configuration, with an unshared s-electron pair and two p bonding orbitals. The bicovalent structure is more favorable for Sn than for Si or Ge because of the higher s-p–hybridization promotional energy due to the increased s-p atomic splitting in the sequence C, Si, Ge, Sn, and Pb; such a configuration is an integral component of the white-tin phase, and exists in a variety of Sn compounds.[27] Evidently, in order for a Sn adatom to bond to two Si surface atoms equivalently, its adsorption position is a bridge site between two dimer pairs as shown in Fig. 8(a). These adsorption positions are randomly distributed for $\Theta < 0.2$ ML to form a two-dimensional gas (Fig. 1), which explains the growing disorder for increasing coverages in this range.

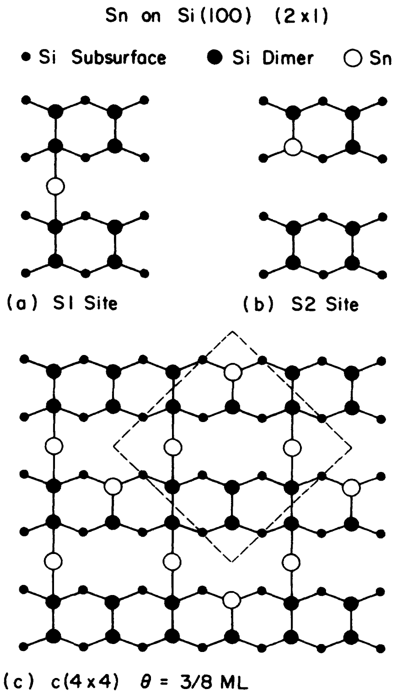

FIG. 8. A picture of structural models for Sn adsorbed on Si(100). This top view of the (100) surface shows the first subsurface Si atomic layer (•), Si dimer- atoms (●), and Sn adatoms (○). The $S1$- and $S2$-site configurations are illustrated in (a) and (b), respectively. A fully developed $c(4\times4)$ is shown in (c).

B. The Sn-Si interaction at higher coverages

The $S2$-site population becomes a significant fraction of the total Sn coverage for $\Theta > 0.2$ ML. The $S2$ sites differ from the $S1$ sites in two fundamental ways. First, the core binding energies of the $S2$ sites appear to follow the position of the VBM for all coverages, while the $S1$-site binding energies remain roughly constant with respect to the Fermi level (Fig. 3). Secondly, there is a large core binding-energy shift between the two sites (0.75 eV for the lowest Sn coverages). Since interdiffusion into bulk Si is negligible, the first finding suggests that the $S2$ emission results from Sn atoms preferentially replacing the surface Si atoms located in the dimerized layer. Once a Sn atom becomes incorporated into the Si lattice, it can be considered as an impurity and its local electrostatic potential should follow that of the Si crystal. Thus its core-level binding energy is tied to the Si VBM in the same way as the Si core level is tied to the Si VBM, independent of the changes in band bending. The Sn $S2$ replacement sites are illustrated in Fig. 8(b); the bonding configuration is tetracovalent with three Sn-to-Si bonds and one dangling bond. The tetracovalent bonding configuration of Sn is found in solid grey tin and many Sn compounds. Similar replacements of group-IV substrate atoms with group-IV adatoms have been observed in related systems.[21,28] With each Si surface atom replaced by a Sn atom, the number of Si atoms exhibiting the -0.5-eV core-level shift is reduced by 1. Thus, the Sn-Si modification number is 1 for the $S2$ site. Since the $S2$-to-$S1$ site population ratio is about 1:2 for $0.2 < \Theta < 0.5$ ML, the average Sn-Si modification number becomes somewhat less than 2 (about 1.7), which is consistent with the experimental result shown in Fig. 4.

The attribution of sites $S1$ and $S2$ with bicovalent and tetracovalent bonding configurations, respectively, qualitatively explains the direction of the core shifts between the two sites following a simple argument based on electrostatics. The increased coordination number of $S2$ relative to $S1$ results in a decrease in electron localization about the atom, and hence an increase in core-level binding energy. The same trend is observed for the surface core-level shift for clean Si(100) (2×1), where the surface atom with a smaller coordination number relative to the bulk atom shows a smaller core-level binding energy.

The observed evolution of the $S1$ core-level binding energy as a function of Sn coverage indicates that the atomic cores of the $S1$ sites are located outside the interface barrier, and therefore the core-level binding energies are not tied to the Si VBM. This is consistent with our interpretation that the $S1$ sites are situated above the Si lattice, and it is expected that for this nearly covalently bonded abrupt interface, the potential barrier is mainly located in a region below the first Sn atomic layer and extending into the Si substrate. The $S1$ binding energy, as discussed above, is roughly a constant relative to the Fermi level. If the Sn-Sn interaction is small, the local work function should change negligibly and the $S1$ core-level binding energy should be roughly tied to the local vacuum level, independent of the band bending. Thus, the observed behavior for the $S1$ binding energy seems to indicate that the net effect from the Sn-Sn interaction is small in this case.

C. Structural implications for ordered Sn on Si(100)

As discussed above, the Sn atoms occupy two inequivalent sites shown in Figs. 8(a) and 8(b). With these basic structural units, one can construct reasonable structural models that are consistent with the phase diagram shown in Fig. 1 and the $S1$-$S2$ site distribution shown in Fig. 6. The Sn-Si modification number has already been explained above and is independent of the details of the reconstruction. For most of the reconstructions, several structural models can be proposed due to the relatively large unit-cell size. Instead of enumerating all possibilities, we will consider here one possible model for a fully developed $c(4\times4)$ corresponding to $\Theta = 3/8$ ML, shown in Fig. 8(c). The model exhibits a basis of three Sn atoms, with two $S1$-type atoms and one $S2$-type atom. The ratio of sites $S2$ and $S1$ is 1:2, consistent with the result in Fig. 6. A $c(4\times4)$ unit cell is indicated by the dashed lines. Note that by simply changing the $S2$-atom location within the unit cell to other sites, one can generate other equally consistent structural models. The number of possible structures increases for the (6×2) and $c(8\times4)$ as the unit-cell size becomes larger, as the readers can easily verify.

For $\Theta \gtrsim 1$ ML, most of the Sn atoms occupy the $S1$ sites. The (5×1) reconstruction represents a significant contraction of the unit-cell size. To fit all of the Sn atoms on the surface, additional Sn—Si bonding probably occurs through the breaking of the Si—Si dimer bond. Owing to the roughly 20% increase in the atomic radius of Sn over Si, a (1×1) Sn structure bonded to an unreconstructed Si substrate at $\Theta = 1$ ML would result in large surface strains, making this structure unfavorable. It is plausible that the $S2$ sites in this structure tend to lessen the strain of long chains of $S1$-like Sn atoms by periodically replacing Si atoms situated in the first Si surface layer; the resulting buckling of the $S1$-like Sn atom chains provides the mechanism for strain relief.

V. SUMMARY AND CONCLUSIONS

The low-coverage Sn-induced $c(4\times4)$, (6×2), $c(8\times4)$, and (5×1) reconstructions on Si(100) have been probed with a high-resolution synchrotron photoemission study. Both the Si $2p$ and Sn $4d$ core levels have been quantitatively analyzed in a manner which yields detailed information concerning the modification and formation of specific sites underlying the Sn-induced reconstructions on Si(100). The Sn $4d$ core-level spectra reveal the presence of two inequivalent sites on the surface. The $S2$ site is seen to remain constant in binding energy with respect to the Si VBM, independent of band bending, while the $S1$ site is seen to roughly follow the Fermi level. By examining the relative energy shifts and emission intensities of both the Sn and Si core levels, the Sn-Si interaction as well as the basic structures of the $S1$ and $S2$ sites is deduced. The Schottky-barrier height is obtained, and the DOS is measured. The basic structural features for the various reconstructions are discussed.

ACKNOWLEDGMENTS

This material is based upon work supported by the U.S. Department of Energy, Division of Materials Sciences, under Contract No. DE-AC02-76ER01198. Some of the personnel and equipment support was also derived from grants from the National Science Foundation (Grant Nos. DMR-83-52083 and DMR-86-14234), the IBM Research Center (Yorktown Heights), the 3M Company, the Hewlett-Packard Laboratories, and the E. I. du Pont de Nemours and Company. The Synchrotron Radiation Center of the University of Wisconsin–Madison is supported by the National Science Foundation under Contract No. DMR-80-20164. We acknowledge the use of central facilities of the Materials Research Laboratory of the University of Illinois, which is supported by the U.S. Department of Energy, Division of Materials Science, under Contract No. DE-AC02-76ER01198, and the National Science Foundation under Contract No. DMR-86-12860.

---

[*] Permanent address: Synchrotron Radiation Research Laboratory, Taipei, Taiwan 107, Republic of China.

[1] R. Farrow, D. S. Robertson, G. M. Williams, A. G. Cullis, G. R. Jones, I. M. Young, and P. J. Dennis, J. Cryst. Growth **54**, 507 (1981).

[2] M. Asai, H. Ueba, and C. Tatsuyama, J. Appl. Phys. **58**, 2577 (1985).

[3] R. E. Schlier and A. T. Farnsworth, J. Chem. Phys. **30**, 917 (1959).

[4] J. Lander and J. Morrison, J. Chem. Phys. **37**, 729 (1962).

[5] M. J. Cardillo and G. E. Becker, Phys. Rev. Lett **40**, 1148 (1978).

[6] J. Ihm,M. L. Cohen, and D. J. Chadi, Phys. Rev. B **21**, 4592 (1980).

[7] P. Kruger, A. Mazur, J. Pollman, and G. Wolfgarten, Phys. Rev. Lett. **57**, 1468 (1986).

[8] K. C. Pandey, in *Proceedings of the 17th International Conference on the Physics of Semiconductors,* edited by D. J. Chadi and W. A. Harrison (Springer-Verlag, New York, 1985), pp. 55–58.

[9] R. J. Hamers, R. M. Tromp, and J. E. Demuth, Phys. Rev. B **34**, 5343 (1986).

[10] J. A. Martin, D. E. Savage, W. Moritz, and M. G. Lagally, Phys. Rev. Lett. **56**, 1936 (1985).

[11] N. Kuwata, T. Asai, K. Kimura, and M. Mannami, Surf. Sci. **143**, L393 (1984).

[12] K. Ueda and K. Kinoshita, Surf. Sci. **145**, 261 (1984).

[13] T.-C. Chiang, CRC Crit. Rev. Solid State Mater. Sci. (to be published).

[14] See, for example, W. F. Egelhoff, Jr., Surf. Sci. Rep. **6**, 253 (1987).

[15] D. E. Eastman and F. J. Himpsel, J. Vac. Sci. Technol. **20**, 609 (1982).

[16] D. H. Rich, A. Samsavar, T. Miller, H. F. Lin, T.-C. Chiang, J.-E. Sundgren, and J. E. Greene, Phys. Rev. Lett. **58**, 579 (1987).

[17] F. R. McFeely, J. F. Morar, N. D. Shinn, G. Landgren, and F. J. Himpsel, Phys. Rev. B **30**, 764 (1984).

[18] G. Hollinger and F. J. Himpsel, Phys. Rev. B **28**, 3651 (1983).

[19] S. L. Hulbert, J. P. Stott, F. C. Brown, and N. Lien, Nucl. Instrum. Methods **208**, 43 (1983).

[20] F. J. Himpsel, P. Heimann, T.-C. Chiang, and D. E. Eastman, Phys. Rev. Lett. **45**, 1112 (1980).

[21] T. Miller, T. C. Hsieh, and T.-C. Chiang, Phys. Rev. B **33**, 6983 (1986).

[22] F. J. Himpsel, G. Hollinger, and R. A. Pollak, Phys. Rev. B **28**, 7014 (1983).

[23] D. H. Rich, T. Miller, and T.-C. Chiang, Phys. Rev. B **37**, 3124 (1988).

[24] K. Takayanagi, Y. Tanishiro, S. Takahashi, and M. Takahashi, Surf. Sci. **164**, 367 (1985).

[25] F. J. Himpsel and D. E. Eastman, J. Vac. Sci. Technol. **16**, 1297 (1979).

[26] A. L. Wachs, T. Miller, T. C. Hsieh, A. P. Shapiro, and T.-C. Chiang, Phys. Rev. B **32**, 2326 (1985).

[27] C. A. Coulson, *Valence* (Oxford University Press, London, 1958), p. 290.

[28] S. B. DiCenzo, P. A. Bennett, D. Tribula, P. Thiry, G. K. Wertheim, and J. E. Rowe, Phys. Rev. B **31**, 2330 (1985).